Chiral metallo-helical complexes enantioselectively target amyloid β for treating Alzheimer's disease

Meng Li,[1] Suzanne E. Howson,[2] Kai Dong,[1] Nan Gao,[1] Jinsong Ren,[1] Peter Scott,[2] and Xiaogang Qu*[1]

[1]Laboratory of Chemical Biology, Division of Biological Inorganic Chemistry, State Key Laboratory of Rare Earth Resource Utilization, Changchun Institute of Applied Chemistry, University of Chinese Academy of Sciences, Chinese Academy of Sciences, Changchun, Jilin 130022, China. E-mail: xqu@ciac.ac.cn

[2]Department of Chemistry, University of Warwick, Gibbet Hill Road, Coventry CV4 7AL, UK

Supporting Information Placeholder

ABSTRACT: Stereochemistry is a very important issue for pharmaceutical industry and can determine drug efficacy. Design and synthesis of small molecules, especially chiral molecules, which selectively target and inhibit amyloid (Aβ) aggregation represent valid therapeutic strategies for treatment of Alzheimer's disease (AD). Herein we report that two triple-helical dinuclear metallo-supramolecular complexes can act as a novel class of chiral amyloid-β inhibitors. Through targeting α/β-discordant stretches at the early steps of aggregation, these metal complexes can enantioselectively inhibit Aβ aggregation, which are demonstrated using fluorescent living cell-based screening and multiple biophysical and biochemical approaches. To the best of our knowledge, there is no report to show that a chiral compound can enantioselectively inhibit Aβ aggregation. Intriguingly, as a promising candidate for AD treatment, the chiral metal complex can cross the blood-brain barrier (BBB) and have SOD activity. Previous studies have demonstrated that chiral discrimination between enantiomers is extremely important, as stereopure drugs can often reduce the total dose of drug given and minimize any toxicity resulting from the inactive enantiomer. And this is also a critical factor which should be carefully considered in AD treatment. Our work provides new insights into chiral inhibition of Aβ aggregation and opens a new avenue for design and screening of chiral agents as Aβ inhibitors against AD.

INTRODUCTION

Alzheimer's disease (AD) is the most common form of dementia, which afflicts more than 24 million people worldwide.[1, 2] A significant body of data has indicated that polymerization of amyloid-β peptide (Aβ) into amyloid fibrils is a critical step in the pathogenesis of AD.[3-7] Therefore, inhibition of Aβ aggregation has been considered as attractive therapeutic and preventive strategy for AD treatment. Although considerable progress has been achieved in discovering inhibitors of Aβ aggregation and toxicity[8-10], chiral recognition of Aβ and aggregation morphology can provide more information on Aβ effects involved in AD pathogenesis, and there is no report to show a chiral compound which has enantioselectivity on targeting and inhibiting Aβ aggregation[11]. Previous studies have demonstrated that chiral discrimination between enantiomers is extremely important especially in the treatment of cancer or neurodegenerative diseases, as stereopure drugs can often reduce the total dose of drug given and minimize any toxicity resulting from the inactive enantiomer.[12, 13] Therefore, chiral discrimination between enantiomers should be a critical factor to be considered in AD treatment.

It has been suggested that the amino acid sequence of $A\beta_{16-23}$, harboring a so-called discordant α-helix, has a strong statistical preference for β-strand structure, and forms a β-strand in Aβ fibrils[14]. Owing to the critical role of α/β discordance in Aβ fibril formation, we and others[15, 16] recent demonstrated that targeting the α-helical form of this region of the Aβ peptide could be a novel approach for designing and screening inhibitors of Aβ aggregation. For the chirality of α-helical structure and the L-amino acids that comprise the peptides, Aβ is sensitive to a chiral environment and the interaction between Aβ and the chiral inhibitor would exhibit a specific orientation[17]. Chiral supramolecular complexes which are suitable for binding and targeting α-helical form of the 16–23 region may show enantioselective effect on inhibiting Aβ fibrillation.

Herein, to achieve chiral recognition of Aβ, we strategically prepared thermodynamically stable single enantiomers of monometallic units[18-20] connected by organic linkers, $[Fe_2L^1_3]Cl_4$ (Λ_{Fe},S_C-$[Fe_2L^1_3]Cl_4$ and Δ_{Fe},R_C-$[Fe_2L^1_3]Cl_4$) and $[Fe_2L^2_3]Cl_4$ (Λ_{Fe},R_C-$[Fe_2L^2_3]Cl_4$ and Δ_{Fe},S_C-$[Fe_2L^2_3]Cl_4$), to enantioselectively target and inhibit Aβ aggregation. This highly adaptable self-assembly approach enables rapid preparation of ranges of water-stable, helicate-like compounds with high stereochemical purity. Both $[Fe_2L^1_3]Cl_4$ (complex **1**) and $[Fe_2L^2_3]Cl_4$ (complex **2**) commonly comprise a chiral assembly of three ditopic bidentate organic ligands around two metal centers (Figure S1). With a diameter of ~1.2 nm (similar to that of a typical α-helix peptide), these metal complexes can be promising candidates for enantioselective inhi-

bition of Aβ fibrillation (Scheme 1). To the best of our knowledge, this is the first example to show that one of the enantiomers can selectively target and inhibit Aβ aggregation.

Scheme 1. Representative illustration of chiral metallosupramolecular complexes enantioselectively bound to Aβ.

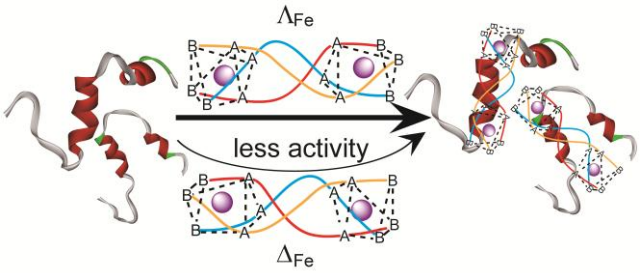

METHODS

Construction of Aβ-ECFP fusion system. The Aβ-ECFP fusion system we constructed was similar to that previously reported by Hecht and co-workers[22]. The Aβ1-42 and ECFP coding sequences were incorporated together by a short linker DNA. *E. coli* strain BL21 (DE3) was transformed by the vector (Aβ-linker-ECFP) or the control vector (linker-ECFP), and cultured at 37℃ in LB media containing 50 mg ml^{-1} ampicillin. Metallo-supramolecular complexes with different concentrations were added to the culture 30 minutes prior to the protein expression induced by 1 mM isopropyl-β-D-thio-galactoside (IPTG). After the expression of the recombinant proteins for 3 hours, all the samples were diluted to 0.1 OD at 600 nm. Fluorescence measurements were carried out by using a Jasco-FP6500 spectrofluorimeter. The excitation wavelength was 433 nm.

Peptide preparation. Aβ25-35 (lot no. 70K49532) and Aβ12-28 (lot no. 32K12201) were purchased from Sigma and Aβ1-40 (lot no. U10012) was obtained from American Peptide. The peptides prepared as described previously[16, 21]. Briefly, the peptide was dissolved in HFIP at a concentration of 1 mg ml^{-1} with shaking at 4 ℃ for 4 hours in a sealed vial for further dissolution. It was then stored at -20 ℃ as a stock solution. Before experiments, the solvent HFIP was removed by evaporation under a gentle stream of nitrogen and peptide was dissolved in aggregation buffer (10 mM HEPES, 150 mM NaCl, pH 7.3). For the preparation of fibrils (fAβ), Aβ1-40 or Aβ25-35 solutions were incubated at 37 ℃ for 7 days.

ThT binding fluorescence. At different times, all Aβ1-40 aliquots in the absence or presence of metal complexes were diluted 80-fold for ThT binding assay using a Jasco-FP6500 spectrofluorimeter. The final concentration of ThT is 10 μM. The excitation wavelength was 444 nm and the emission intensity at 482 nm was used for analysis.

Atomic Force Microscope (AFM) imaging. 50 μM Aβ1-40, and 50 μM Aβ1-40 in the presence of equimolar complex **1** or complex **2** were incubated for 7 days at 37 ℃. Samples were prepared as described previously[16, 21]. Briefly, samples were diluted with deionized H_2O to yield a final concentration of 1 μM. Then aliquots of 50 μL of each sample were placed on a freshly cleaved mica substrate. After incubation for 5 min, the substrate was rinsed twice with water and dried before measurement. Tapping mode was used to acquire the images under ambient condition.

Circular dichroism (CD) measurements. CD spectra were collected at 37 ℃ with a JASCO J-810 spectropolarimeter using a 1 mm path length quartz cell. The parameters were controlled as 0.1 nm intervals, 4 seconds response, and each sample was an average of three scans in a speed of 5 nm min^{-1} over the wavelength range from 200 nm to 250 nm.

Sedimentation and electrophoresis assay. Aβ1-40 peptide (50 μM) in the absence or presence of 50 μM metal complexes was incubated at 37 ℃ for 7 days. The aggregated peptide in each sample was separated by centrifugation at 13500 rpm for 20 min at 20 ℃. The pellets were resuspended and boiled after the addition of sample buffer. Samples were run on a 12% Tris–tricine SDS gel at 100 V for 1 hour, followed by silver staining.

Trypsin digestion. Aβ12-28 (10 μL, 20 μM) was incubated at 37 ℃ for 1 h with trypsin (0.1 mg ml^{-1}) in the absence or presence of increasing concentrations of complex **2**. At the end of the reaction, all samples were supplemented with SDS-PAGE reducing sample buffer, and heated at 100 ℃ for 5 min. Gels were run in a Tris/Tricine system after which the gels were silver-stained. Lysozyme, which can also be digested by trypsin, was used as control.

NMR Spectroscopy. Samples for NMR were run in aqueous Tris buffer with 10% ^2H_2O added. Samples containing Aβ1-40 were run at 0.1 mM. The metal complexes (Λ_{Fe},Rc-$[Fe_2L^2_3]Cl_4$ and Δ_{Fe},Sc-$[Fe_2L^2_3]Cl_4$) were incubated with Aβ1-40 at 37 ℃ for 2 h. NMR measurements were carried out on a Bruker 600-MHz AVANCE NMR spectrometer equipped with a triple channel cryoprobe at 5 ℃. The concentrations of the metal complexes were 0.1 mM.

Docking studies. Flexible ligand docking studies were performed using AutoDock Vina. Metal Complexes (Λ_{Fe},Rc-$[Fe_2L^2_3]Cl_4$ and Δ_{Fe},Sc-$[Fe_2L^2_3]Cl_4$) were created using PyMOL and studies were conducted against the Aβ1-40 monomer (aqueous solution NMR structure, PDB 2LFM). The structures for these metal complexes and Aβ1-40 were prepared for use with AutoDock Vina using AutoDock Tools. All hydrogens were added to Aβ1-40 and the peptide was contained within a search space sized to contain the whole monomer. No modifications were made to the metal complexes, and torsions were kept as the default selected in AutoDock Tools.

Reactive oxygen species detection. PC12 cell (Rat pheochromocytoma, American Type Culture Collection) cultures grown on 24-well plateswere incubated with 50 μM 2′,7′-dichlorofluorescin (DCF) diacetate (Beyotime, China) for 30 min at 37 ℃ after 12 h with samples. The cells were then rinsed with PBS solution. Intracellular esterases convert DCF diacetate to anionic DCFH which is trapped in the cells. The fluorescence of DCF, formed by the reaction of DCFH with ROS was examined with a spectrofluorometer (JASCO-FP6500, Japan).

SOD Activity Determination. The SOD activities of these metal complexes were assayed by measuring inhibition of the photoreduction of nitro blue tetrazolium (NBT), by a method slightly modified from that originally described by Beauchamps and Fridovich. The solutions containing riboflavin (20 μM), methionine (0.013 M), NBT (75 μM), and metal complex of various concentrations were prepared with 50 mM phosphate buffer (pH 7.8). The mixtures were illuminated by a lamp with a constant light intensity for 10 min at 25 ℃. After illumination, immediately the absorbance was measured at 560 nm. The entire reaction assembly was enclosed in a box lined with aluminum foil. Identical tubes with the reaction mixture were kept in the dark and served as blanks. Inhibition

percentage was calculated according to the following formula: % inhibition = $[(A_o - A)/A_o] \times 100$, where A_o is the absorbance of the control and A is the absorbance of the samples.

Cell culture and neurotoxicity assay. PC12 cells (Rat pheochromocytoma, American Type Culture Collection) were maintained in Iscove's modified Dulbecco's medium (IMDM) (Gibco, BRL) supplemented with 5% Fetal bovine serum and 10% heat inactivated horse serum at 37 ℃ in a humidified atmosphere of 5% CO_2 and 95% air. Differentiation was induced by 50 μg ml^{-1} nerve growth factor (NGF) (invitrogen) until about 80% cells extended neuronal-like processes. Cells were plated at 30 000 cells per well on poly-L-Lysine coated 96-well plates in fresh medium. After 24 hours, Aβ1-40 peptides (5 μM) that had been aged with or without various concentrations of metal complexes were dispensed into the PC 12 cells, and the cells were further incubated for 36 hours at 37 ℃. Cytotoxicity was measured by using a modified MTT assay Kit (Promega). Absorbance values of formazan were determined at 490 nm with an automatic plate reader. All tests were repeated three times in quadruplicate wells.

Assay of intracellular free calcium. PC12 cells were plated at a density of 3×10^5 cell/mL on glass overslips coated with poly-L-lysine. Two days later, the cells, when at approximately 80% confluence, were exposed to either Aβ or Aβ plus the metal complexes for 2 hours. Cells were then washed and fixed with paraformaldehyde (4%) for 10 minutes at room temperatures. Fixed cells were incubated at 37℃ for 1 hour in IMDM-serum free media containing 3 μM Fluo-3 AM (Beyotime, China). Fluorescence from Fluo-3 AM was captured using flow cytometry. The excitation wavelength was 488 nm.

RESULTS AND DISCUSSION

By using a high-throughput screening method based on the fluorescence of an Aβ-enhanced cyan fluorescent protein (ECFP) fusion expression system constructed in our laboratory[16, 21, 23] which was originally developed by Hecht and co-workers[22], we have identified the two pairs of metal complexes capable of inhibiting Aβ aggregation (Figure 1A). ECFP folds into its native state slowly and the fluorescence of the Aβ-ECFP fusion depends on Aβ folding and solubility. Aβ aggregation can lead to the entire Aβ-ECFP fusion to misfold and not to emit fluorescence. Inhibitors that can block or retard Aβ aggregation would enable ECFP fold into native structure to recover its fluorescence. Figure 1B unambiguously indicated that all of these metal complexes could strongly inhibit Aβ aggregation. In the presence of these metal complexes, metal complex concentration-dependent fluorescence enhancement was observed. The complex **1** had significantly higher inhibition activity compared to complex **2**. Further study demonstrated that enantiomers Λ**1** (Λ_{Fe},Sc-$[Fe_2L^1_3]Cl_4$) and Λ**2** (Λ_{Fe},Rc-$[Fe_2L^2_3]Cl_4$) exhibited higher inhibition effects on Aβ aggregation than their mirror image Δ**1** (Δ_{Fe},Rc-$[Fe_2L^1_3]Cl_4$) and Δ**2** (Δ_{Fe},Sc-$[Fe_2L^1_3]Cl_4$), respectively. Importantly, the enantioselectivity of complex **2** was even more obvious than complex **1**. Control experiments showed that almost no fluorescence enhancements were observed for the non-Aβ fusion system (Figure S2), indicating that the fluorescence enhancements were not due to the interactions of these complexes with the fluorescent protein.

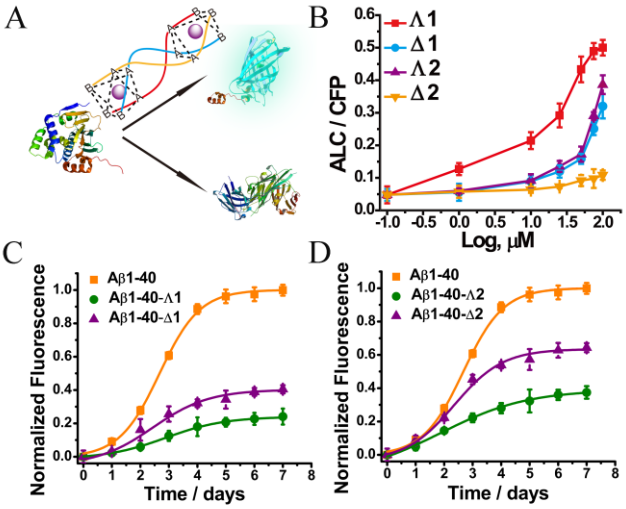

Figure 1. (A) Schematic representation of screening Aβ aggregation inhibitors using Aβ-linker-ECFP fusion screen system. (B) Screening results from the screen system. The inhibition effect of metal complexes showed both structural and chiral selectivity. Fibrillation kinetics of Aβ1-40 as monitored by the development of thioflavin T binding in the absence or presence of (C) complex **1** and (D) complex **2**. Aβ1-40 concentration was 50 μM and the metal complexes concentrations were 10 μM. The samples were measured in 10 mM HEPES (pH 7.3) after incubation at 37℃ for 7 days.

To verify the chiral effect of these metal complexes on the assembly of Aβ1-40 into amyloid fibrils, we employed commonly used thioflavin T (ThT) fluorescence assay (Figure 1C and 1D). ThT, an extrinsic fluorescent dye, is able to bind to amyloid fibrils; upon binding, its fluorescence intensity increases.[24-26] When fresh Aβ1-40 alone was incubated at 37℃, ThT fluorescence showed a sigmoidal shape as a function of incubation time (Figure 1C). This result was consistent with the nucleation-dependent polymerization model. However, all these metal complexes can decrease ThT fluorescence in a dose-dependent manner (Figure S3). IC_{50} values were estimated to be 1.69 μM for Λ**1**, 5.43 μM for Δ**1**, 6.62 μM for Λ**2** and 42.2 μM for Δ**2** (Table 1). In control experiments, metal complex alone did not influence ThT fluorescence under our experimental conditions (Figure S4). These preliminary IC_{50} data indicated two trends in the anti-aggregation activity of the flexicates. First, systems with less polar ligands (complex **1**) were more effective. Second, the Λ_{Fe} enantiomers showed more effective activities than the Δ_{Fe} enantiomers. Furthermore, the decreased ThT fluorescence almost reached maximum at the equal concentration of metal complex (Figure S3), indicating that Aβ1-40 possibly interacted with the metal complexes at 1:1 ratio, which was consistent with previous studies[27]. As indicated by their work[27], 1:1 binding suggested that the inhibition occurred at a very initial stage of the aggregation process[24-26]. That was to say that these metal complexes could target the Aβ monomers to inhibit the formation of the early soluble Aβ oligomers which were reported to be more toxic and responsible for the neurotoxicity in AD than the extracellular insoluble Aβ deposits.[28, 29]

For further confirming the inhibition effect of these metal complexes on Aβ aggregation, sodium dodecyl sulfate (SDS)-PAGE assay was used[30, 31]. After incubation for 7 days, the large molecular weight Aβ1-40 aggregates were separated from the low molecular Aβ species by spinning down the samples. The aggregated peptide pellets were resuspended and boiled after addition of sample buffer, and were run on the SDS-PAGE to check the total amounts of aggregated Aβ. Our results showed that after incubation with complex **1** and **2**, the quantity of the resuspended peptide was significantly decreased, especially for Λ**1** (Figure S5), indicating that these metal complexes could inhibit Aβ aggregation.

We also investigated the effect of these metal complexes on the morphology of Aβ1-40 aggregates using atomic force microscopy (AFM)[32-34]. As shown in Figure 2A, classical amyloid fibrils were observed in samples of untreated Aβ1-40. The Aβ1-40 fibrils were non-branched, helical filaments with diameters of ~10 nm and lengths of up to several microns. When incubated with the metal complexes, especially with Λ**1**, numerous small, relatively amorphous aggregates were observed, demonstrating the excellent efficacy of metal complexes to inhibit Aβ1-40 aggregation (Figure 2A and Figure S6). Aβ oligomers, protofibrils and fibrils all share the common β-sheet structure which drives Aβ aggregation and toxicity. Circular dichroism studies (Figure 2B and 2C) indicated that all these metal complexes could inhibit structural transition from native Aβ1-40 random coil to β-sheet conformation in solution. Our inhibition data further demonstrated that these two metallo-supramolecular complexes could inhibit Aβ self-assembly at the early steps, in agreement with the cell-based screening results, ThT fluorescence and AFM data.

Intriguingly, ligand L (both R and S) alone showed little inhibition effects and chiral discrimination on Aβ aggregation (Figure S7). When assembled into triple helicate metallo-supramolecular structure, these metal complexes could not only inhibit Aβ aggregation but also destabilize preformed fibril (Figure S8 and Table 1) with enantioselectivity. Upon Aβ1-40 binding, the spectral position and intensity of the metal-to-ligand charge-transfer (MLCT) bands of the metallo-supramolecular complex did not change (Figure S9), indicating that Aβ binding did not destroy the metal complex rigid structure[18-20].

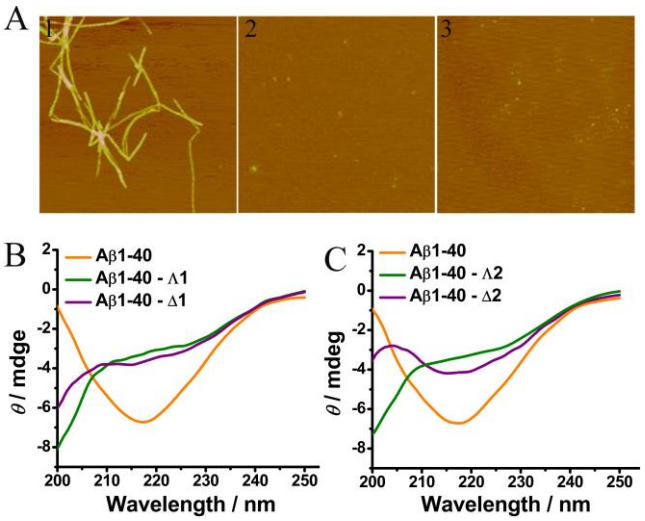

Figure 2. (A) The morphology of Aβ1-40 aggregates was analyzed by AFM images (area corresponding to 2.5 μm × 2.5 μm). 1) 50 μM Aβ1-40. 2) 50 μM Aβ1-40 in the presence of 50 μM complex Λ**1**. 3) 50 μM Aβ1-40 in the presence of 50 μM complex Δ**1**. The ability of (B) complex **1** and (C) complex **2** to inhibit Aβ1-40 aggregation was monitored by CD assay. Aβ1-40 concentration was 50 μM and the metal complexes concentrations were 10 μM. The samples were measured in 10 mM HEPES (pH 7.3) after incubation at 37℃ for 7 days.

To further support our enantioselective results, dialysis experiments[35, 36] were designed to reveal the structural selectivity of these metal complex enantiomers. A racemic mixture of complex **1** or complex **2** was prepared by mixing equimolar amounts of the pure enantiomers (Figure 3A and 3B). The racemic mixture was dialyzed against Aβ1-40, and circular dichroism was used to monitor the dialysate for enrichment of the enantiomer with lower binding affinity to Aβ1-40 in the dialysis tube. As shown in Figure 3A and 3B, the dialysate was enriched in Δ**1** and Δ**2**, respectively. These results indicated unambiguously that Λ**1** and Λ**2** bound preferentially to Aβ1-40 compared with their mirror images, respectively.

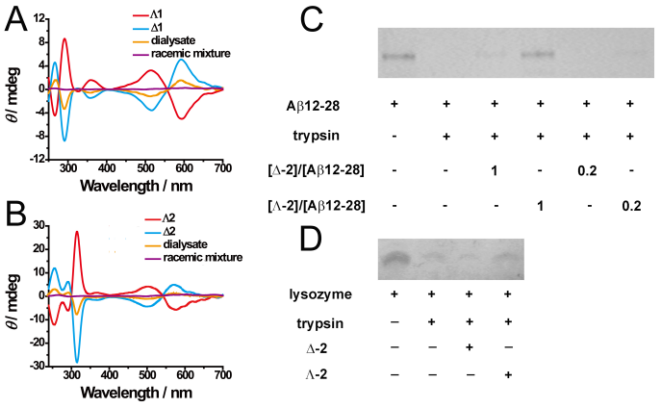

Figure 3. CD spectra of the dialysate for enrichment in the enantiomer with poorer affinity for the Aβ1-40 contained within the dialysis tube in competition dialysis experiment. (A) complex **1**, (B) complex **2**. SDS-PAGE analysis of the effect of complex **2** on tryptic digests of (C) Aβ12-28 and (D)

lysozyme was used as control. Experimental details were described in Materials and methods section.

ESI-MS[28, 29] was also employed to compare the binding ability of the metal complexes to Aβ. Here we took complex **2** as an example since the chiral discrimination between the two enantiomers was more obvious. As shown in Figure S10A, the Aβ1-40 peptide alone gave two peaks at 1083 and 1444, corresponding to the 4+ and 3+ ionization states of the Aβ1-40 monomer, respectively. However, after treatment of Aβ1-40 with complex **2**, extra peaks were observed at 1208 and 1509 in the mass spectrum (Figure S10C and Figure S10D), which corresponded to the 1:1 metal complex-Aβ monomer complex. These results further supported that the metal complexes bound with Aβ peptide in 1:1 binding ratio. Intriguingly, after treatment of the Aβ peptide with Λ**2**, the metal complex fragment peaks in the mass spectrum was weaker than the samples treated with Δ**2**, indicating that Aβ1-40 bound more tightly with Λ**2** to prevent the metal complex to be ionized, which would be supported by our next quantitative fluorescence titration studies.

Table 1 IC_{50} values of complex 1 and complex 2 for inhibition of the fibril formation and destabilization of the preformed fibrils.

	Inhibition (μM)		Destabilization (μM)	
Metal complexes	Aβ1-40	Aβ25-35	Aβ1-40	Aβ25-35
Λ1	1.69±0.23	36.38±4.59	1.97±0.46	41.19±2.94
Δ1	5.43±0.86	> 50	8.53±0.71	> 50
Λ2	6.62±0.58	> 50	9.82±1.23	> 50
Δ2	42.21±6.13	> 50	> 50	> 50

The four metal complexes showed different inhibition abilities. To gain better understanding of the inhibition effects of the metal complexes, we compared the binding affinity of the four metal complexes to Aβ1-40 by using fluorescence titrations method[39, 40]. The fluorescence intensity of Aβ1-40 was quenched as increasing the amount of metal complexes. The apparent binding constants (Table 2) yielded by a nonlinear least squares fit which had been corrected for the inner filter effect[41, 42] (Figure S11 and Table 2), were in agreement with the IC_{50} values of the metal complexes against Aβ1-40 aggregation (Table 1). Therefore, we concluded that the different inhibition ability of these given metal complexes depended mainly on the different binding affinity to Aβ1-40. Although complex **1** and complex **2** had a similar triple-helical structure, the two iron cylinders showed different Aβ inhibition activity and binding affinity due to their different ligands. The more flexibly linked complex **2** had a weaker hydrophobic interaction and π-π stacking with the peptide.

On the basis of the above results, we further employed different Aβ fragments, Aβ25-35 and Aβ12-28 to explore the specific metal complex-binding site on Aβ. Previous studies have shown that Aβ25-35 fragment similar with Aβ1-40 can form Aβ fibrils[43-45]. However, under our experimental conditions, both the inhibition and destabilization effects of these metal complexes on Aβ25-35 exhibited much weaker (Figure S8B, S12 and Table 1). The two pairs of metal complexes could not inhibit the aggregation completely even at a very high concentration, indicating that these metal complexes bound weakly to Aβ25-35. The Aβ binding sites of these metal complexes might not locate in the region of Aβ25-35. These metal complexes we studied here has two metal ions with 4 positive charges and three non-planar hydrophobic ligands, and forms a triple helicate rigid structure (diameter 1.2 nm) compatible with peptide α-helical form of the Aβ13-23 region. Aβ13-23 may be a promising binding region for them. To confirm our hypothesis, competitive binding assay using 4,4'-bis(1-anilinonaphthalene 8-sulfonate) (bis-ANS)[46, 21] was employed. Bis-ANS is suitable to study binding site because it can recognize soluble α-helical or random coil/mixed Aβ conformers at acidic pH. The fluorescence intensity of bis-ANS was strongly enhanced upon binding to Aβ1-40. These metal complexes showed competitive binding to Aβ1-40 with bis-ANS. Fluorescence quenching data was fit with the Stern-Volmer equation and yielded the quenching constants of 2.29×10^6 M^{-1}, 1.23×10^6 M^{-1}, 1.29×10^6 M^{-1} and 6.11×10^5 M^{-1} for Λ**1**, Δ**1**, Λ**2** and Δ**2**, respectively (Figure S13A). These results implied that the binding site for the metal complexes was close to that of bis-ANS. As for Aβ12-28, similar competitive binding results were obtained, and the quenching constants were 2.46×10^6 M^{-1}, 1.37×10^6 M^{-1}, 1.50×10^6 M^{-1} and 7.86×10^5 M^{-1} for Λ**1**, Δ**1**, Λ**2** and Δ**2**, respectively (Figure S13B). Therefore, these metal complexes may bind to the Aβ12-28 region, the central hydrophobic domain of Aβ1-40.

Table 2 Binding Constants of different metal complexes with Aβ1-40.

Metal complex	Λ1	Δ1	Λ2	Δ2
Binding constants[a] (M^{-1})	3.81×10^6	9.62×10^5	1.04×10^6	1.97×10^5

[a]Binding constant was measured by fluorescence titration method and yielded by a nonlinear least squares fit which corrected for the inner filter effect. The values were the average of two independent measurements. Experimental details were described in Supporting Information.

To further study the binding site, we carried out digestion experiments with trypsin[16, 21]. Complex **2** was taken as an example. We chose Aβ12-28 as the trypsin substrate; the cleavage site (lysine residues) was just next to the central hydrophobic region. It was clearly shown that complex **2** could prevent the digestion of this fragment (Figure 3C), which indicated that complex **2** did bind to this hydrophobic region of Aβ1-40 peptide. Therefore,

our enzyme digestion experiments, inhibition data, circular dichroism, fluorescence quenching and competitive binding results indicated that these metallo-supramolecular complexes bound to the Aβ central region covering the α/β-discordant stretch of Aβ13-23, which had a similar helical size to the metal complexes.

The above results disclosed a remarkable stereoselective interaction between Aβ and chiral metallo-supramolecular complexes. The benzene rings at the center of the metal complex (Figure S1) are stacked together by face-edge π interactions which forms strong π surface, and aryl lined cavities also have the potential to trap small molecules[12-14]. The aromatic amino acid residues in the central hydrophobic region of Aβ1-40, phenylalanine F19 and F20, can bind to the surface of the central benzene rings of metal complex through hydrophobic interaction and π-π stacking. As for Aβ1-40, the π-π stacking is also one of the most important factors influencing its physical and chemical behaviors[47, 48]. Due to the α-helical structure of the main chain and the chirality of L-amino acids that comprise the peptides, Aβ1-40 would exhibit different hydrophobic interaction and π-π stacking with the Δ/Λ enantiomers. In addition, the positive charges of the two metal centers would not only increase the compounds' solubility but also enhance their binding ability to negatively charged Aβ through electronic interactions.

The binding sites and different binding models between the chiral metal complexes and Aβ1-40 were further confirmed by NMR spectroscopy[49-53]. The ^{1}H NMR signals of the aromatic moieties (F19F20)[49, 50] of Aβ1-40 underwent remarkably change upon addition of complex **2**, revealing their interactions associated with these units (Figure 4A and 4D). The metal complexes can specifically bind to the hydrophobic core fragment of Aβ1-40, which was consistent with our above results. In addition, compared with NMR spectrum of Aβ1-40 alone, there were obvious peak shifts in signals from amide protons of K16 (2.95 ppm), and E22 (2.52 ppm) in the presence of Λ**2** and Δ**2** (Figure 4B and 4C)[52, 53]. The NMR spectrum of the Aβ1-40 in the presence of Λ**2** (Figure 4, blue) was different from that treated with Δ**2**. Λ**2** caused the peaks shifted to the lower field while Δ**2** made them moved to the higher field, suggesting that Λ**2** and Δ**2** bound differently with Aβ1-40 in the 16-23 sequence.

The L-amino acids usually arrange in a specific orientation on the surface of Aβ1-40, making the Aβ1-40 sensitive to a chiral environment.[11, 17] With a triple-helical array structure and comparable in size to Aβ1-40 peptide[18], the metal complex would make the peptide molecules stacking on the surface of the metal complex. Considering the different effects of steric hindrance caused by the large pyridylimine unit and the helical chirality of the metallo-supramolecular complex, the L-amino acids arranged on the surfaces of the Aβ1-40 peptide would exhibit different hydrophobic interaction with the Δ/Λ enantiomers, resulting in obvious different peak shifts in signals from amide protons of K16 and E22 (Figure 4). Therefore, the enantioselective interactions between Aβ1-40 and chiral metallo-supramolecular complexes were due to the high stereospecific binding between these metal molecules and the L-amino acid arranged on the surfaces of the Aβ1-40 peptide.

To better understand and visualize the interactions of metal complexes with the monomeric Aβ1-40 peptide, the metal complex molecules were docked against the previously reported NMR structure of monomeric Aβ1-40 (PDB 2LFM) in an aqueous environment using AutoDock Vina.[23, 54, 55] Although multiple structures of Aβ (PDB 2LFM, 1IYT, 1BA4, 1ZE9, etc.)[54] have been demonstrated, we employed the structure obtained in an aqueous environment to carry out our study. In this condition, the Aβ1-40 peptide contained 3_{10} helix in the central hydrophobic region (residues 13-23) and collapsed in the N- and C-termini.[54] Furthermore, the helical intermediates in early fibrillogenesis events could convert into β structures, which was in agreement with our experimental results. The structures of the Aβ1-40 and metal complexes used to perform the docking studies were shown in Figure S14. Figure 4 provided the low-energy conformations of Aβ1-40-metal complexes. The complex **1** was positioned in the 13-23 region of the Aβ1-40 peptide, further supporting that the metal complexes inhibited Aβ aggregation by blocking the intermolecular interactions of multiple Aβ1-40 molecules. Binding free energy changes were -7.9 and -7.1 kcalmol^{-1} for Λ**1** and Δ**1**, respectively (Table S1), which demonstrated enantioselective interactions between Aβ and chiral metallo-supramolecular complexes, and Λ**1** bound more tightly to Aβ1-40 than Δ**1**. The two enantiomers of complex **2** binding to Aβ were shown in Figure S15, enantioselective interactions were also observed, Λ**2** bound more tightly to Aβ1-40 than Δ**2**. All these simulation results were in agreement with our NMR data, the chiral metal complex bound to the hydrophobic region from K16 to E22.

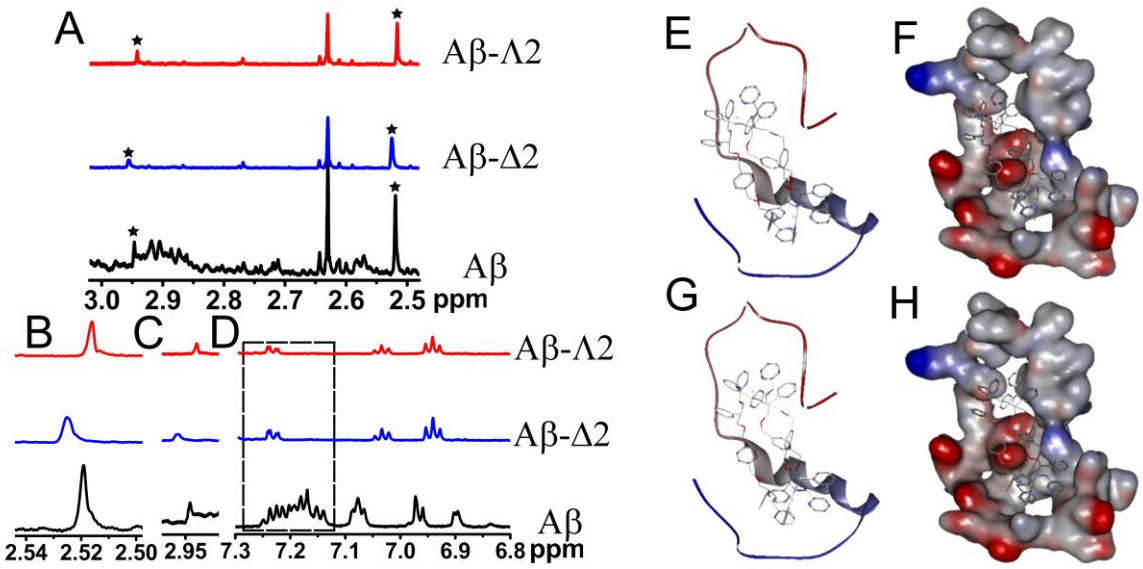

Figure 4. ^{1}H NMR spectra of Aβ1-40 before and after the treatment with the two enantiomers of complex **2**. (A) The signals of Aβ1-40 from amide protons of K16, F19, and E22 showed different shifts (see the peaks marked with asterisks). (B) Locally amplified ^{1}H NMR spectra in Figure 4A centered at 2.52 ppm. (C) Locally amplified ^{1}H NMR spectra in Figure 4A centered at 2.95 ppm. (D) The peaks due to the protons of F19 and F20 (see the box centered at 7.2 ppm) were significantly reduced in intensity after incubation with complex **2**. Signals of Aβ1-40 are assigned based on literature values[49-53]. Energy-minimized average models of Λ**1** (E and F) and Δ**1** (G and H) with Aβ interactions. Cartoon (left) and surface (right) representations of complex **1** interacting with Aβ in the 13-23 region of the Aβ1-40 peptide.

It has been proposed that Aβ can cause signaling amplification that inactivates superoxide dismutase (SOD-2) and generates additional free radicals[56]. Moreover, AD model mice crossed with SOD-2 heterozygous knock out mice exhibited increased plaque deposition and tau phosphorylation in their brain[57]. Administration SOD reduces hippocampal superoxide and prevents memory deficits in a mouse model of AD[58, 59]. The rational design and synthesis of low molecular weight catalysts which mimic the SOD enzyme function possesses promising for use as a human pharmaceutical in the treatment of AD. It is known that certain metal-containing model compounds show catalase and/or SOD activity[60, 61]. Reports have appeared on the SOD-like activity of the iron (ll1) derivative of porphyrin[61]. Considering these facts, we speculated that the iron supramolecular complex we used here may form an active artificial enzyme center and show SOD activity.

The SOD activities of these metal complexes were quantified using a modified nitro blue tetrazelium (NBT) assay system[62, 63]. The NBT assay was based on the capacities of these metal complexes to inhibit the reduction of nitroblue tetrazolium (NBT) by photochemically generated superoxide anion radical in the presence of riboflavin. As shown in Figure 5A, due to the different chiral catalytic center, the metal complexes exhibited enantiodifference to mimic SOD activity. The Λ_{Fe} enantiomers were more effective than the Δ_{Fe} enantiomers.

Next we investigated the effects of the metal complexes on ROS production generated by Aβ1-40 aggregation in PC12 cells, which has been suggested as one proposed mechanism of AD pathogenesis. Our results indicated that the metal complexes could effectively suppress the Aβ1-40-induced ROS production (Figure 5B and 5C). On the basis of these data, these metal complexes could act as not only SOD mimics but also free-radical scavengers.

The ability of these metal complexes to inhibit Aβ assembly suggested that they might be useful in blocking Aβ-mediated cellular toxicity. To address this question, we used differentiated PC12 cells to perform MTT assay to probe cellular metabolism[21, 32-34]. Cells, forced to undergo neuronal differentiation, have been demonstrated to mimic the neurons in the brain and be more sensitive to neurotoxicity of Aβ aggregation than normal PC12 cells[34]. As shown in Figure 5D and 5E, aged Aβ1-40 led to a decrease of 42% in cellular reduction of MTT. Complex **1** or Complex **2** could prevent cell death in a dose-dependent manner. The complex **1** or complex **2** alone, under our experimental conditions and concentration range, had little effect on PC 12 cell viability (Figure S16), showing their low toxicity against PC12 cells. As expected, due to their different binding affinity to Aβ1-40, the Λ_{Fe} enantiomers were more effective than the Δ_{Fe} enantiomers to inhibit Aβ-induced cytotoxicity, which demonstrated that the chiral discrimination of these metal complexes was obvious even in the complex culture medium. However, the complex **1** showed slightly stronger protection effect than complex **2**, indicating that Aβ-induced cytotoxicity was complicated when incubated with Aβ1-40 and the metal complexes together, although the complex **1** had a higher binding affinity to Aβ1-40.

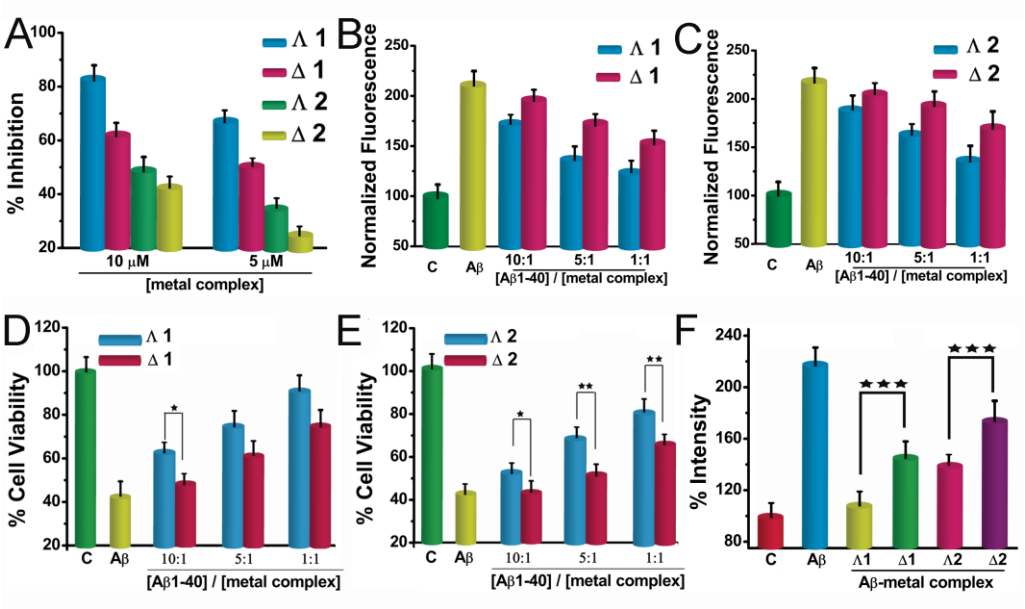

Figure 5. (A) Percentage inhibition of NBT oxidation by superoxide radicals generated in riboflavin-NBT-light system in vitro assessed by NBT^{+} absorption at 560 nm with complex **1** and complex **2**. (B and C) Effect of the metal complexes on ROS production in PC12 cells. Cells were treated with aged Aβ1-40 at a concentration of 5μM in the absence or presence of increasing concentration of metal complexes and 12 h later ROS generation inside the cells was measured using dichlorodihydrofluorescein (DCF) fluorescence. (D and E) Protection effects of metallo-supramolecular complexes on Aβ1-40-induced cytotoxicity of PC 12 cells. The concentration of Aβ1-40 was 5 μM. (F) Inhibition of Aβ-induced calcium uptake by metal complexes. Cells were exposed to 5 μM Aβ1-40 or 5 μM Aβ1-40 pretreated with metal complexes at concentrations of 5 μM. After 2 hours cells were washed, fixed and incubated in medium containing the cell permeant calcium-sensitive dye Fluo-3 AM, as described in methods section. The data points shown are the mean values ± standard error of the mean (SEM) from three independent experiments. *P < 0.05, **P < 0.01, ***P < 0.001. Control: Aβ-untreated cells.

It has been proposed that one of the neurotoxic mechanisms of Aβ is a direct consequence of the ability of Aβ to form calcium channels in the target neurons. Perturbation of calcium homeostasis may also contribute to a self-amplifying cascade of free radical- and Ca^{2+}-mediated degenerative processes which involved in the neurodegenerative phenotype of Alzheimer's disease.[64-66] Effective blocking Aβ formed calcium channel can be critical for protection of the cells from Aβ cytotoxicity. To test the hypothesis that these metal complexes were interfering with Aβ-dependent intracellular calcium change, we used the cell-permeant calcium-sensitive dye Fluo-3 AM to measure intracellular calcium levels in treated cells. As shown in Figure 5F, calcium accumulation into the Aβ-treated cells was substantial and statistically significant in the absence of the metal complexes. In contrast, in the presence of either complex **1** or complex **2**, significant decrease of calcium accumulation was observed. Therefore, these metal complexes interfered with Aβ-induced intracellular calcium change. Importantly, the enantioselectivity of these metal complexes was also obvious. The Λ enantiomers could block the Aβ calcium channel more effectively than the Δ_{Fe} enantiomers.

As suitable candidates for AD treatment, these metal complexes should cross the blood-brain barrier (BBB). To determine whether complex **1** and complex **2** could passively accumulate in the brain of living animals, we used ICP-MS to measure the amount of Fe in the mice brain after intraperitoneal injection for 4 hours. A significant level of Fe was found in the cerebrospinal fluid (CSF) of the mouse that treated with metal complexes compared to the control mouse. The efficiencies of Fe accumulation in the brain were 1.5% and 0.7% for complex **1** and complex **2** respectively, indicating these metal complexes possessed the ability to cross BBB. These results further supported that these metal complexes can act as promising therapeutic agents for AD treatment. Furthermore, compared with complex **1**, complex **2** showed weaker ability to cross the BBB which could be due to the larger size.

It was worth noting that these metal complexes with three-dimensional (3D) structures were comparable in size to Aβ1-40 peptide. Strong attraction between the peptide molecules and metal complexes would result in their stacking on the edges of the metal complexes and concomitant scrambling of the 3D lock-and-key match between the neighbouring peptide molecules[67], which would further inhibit the self-assembly of Aβ1-40 and affect the physiological functions of the Aβ species. Although several compounds that affect Aβ polymerization have been identified via different approaches[8-10], these compounds show the inhibition effects only in their racemic form and lack stereospecific binding interactions with Aβ, owing to their smaller size or nonspecific binding manner. The present investigation suggests that targeting the central α-helix of monomeric Aβ peptide by

the large synthetic multiple cationic arrays with a similar size of α-helix peptide can offer an effective approach to demonstrate the specific effect of chirality of the Aβ inhibitors on the inhibition of Aβ self-assembly. Polyvalency is a powerful means for designing ligands that bind more strongly to targets[68, 69]. Attachment of the metal complexes, in a stable way and active structural conformation, on the surface of biocompatible/biodegradable and stealth nanoparticles may increase the binding affinity of metal complexes for Aβ peptides and amplify the role of chirality in the interaction between metal complexes for Aβ peptides, due to the multivalency.

CONCLUSIONS

In summary, two triple-helical dinuclear metallosupramolecular complexes have been identified as a novel class of chiral amyloid-β inhibitors. Through targeting α/β-discordant stretches at the early steps of aggregation, these chiral metal complexes can enantioselectively inhibit Aβ aggregation, which are demonstrated using fluorescent cell-based screening and multiple biophysical and biochemical approaches. To the best of our knowledge, there is no report to show that one of the enantiomers can selectively inhibit Aβ aggregation. It is well known that chiral discrimination between enantiomers is extremely important, as stereopure drugs can often reduce the total dose of drug given and minimize any toxicity resulting from the inactive enantiomer. Therefore, chiral discrimination between enantiomers is a critical factor to be considered in AD treatment. Our work may open a new avenue for design and screening of chiral supramolecular complexes as Aβ inhibitors against AD.

ASSOCIATED CONTENT

Supporting Information. Experimental details and characterization data. This material is available free of charge via the Internet at http://pubs.acs.org.

Corresponding Author

xqu@ciac.ac.cn

ACKNOWLEDGMENTS

This work was supported by 973 Project (2011CB936004, 2012CB720602), and NSFC (21210002, 91213302).

REFERENCES

(1) Blennow, K.; de Leon, M. J.; Zetterberg, H. *Lancet* **2006**, *368*, 387-403.
(2) Rauk, A. *Chem. Soc. Rev.* **2009**, *38*, 2698-2715.
(3) Jakob-Roetne, R.; Jacobsen, H. *Angew. Chem. Int. Ed.* **2009**, *48*, 3030-3059.
(4) Gaggelli, E.; Kozlowski, H.; Valensin, D.; Valensin, G. *Chem. Rev.* **2006**, *106*, 1995-2044.
(5) Hamley, I. W. *Chem. Rev.* **2012**, *112*, 5147-5192.
(6) Cassagnes, L. E.; Herve, V.; Nepveu, F.; Hureau, C.; Faller, P.; Collin, F. *Angew. Chem.* **2013**, *125*, 11316-11319.
(7) Pedersen, J. T.; Hureau, C.; Hemmingsen, L.; Heegaard, N. H. H.; Ostergaard, J.; Vasak, M.; Faller, P. *Biochemistry* **2012**, *51*, 1697-1706.
(8) Yang, F.; Lim, G. P.; Begum, A. N.; Ubeda, O. J.; Simmons, M. R.; Ambegaokar, S. S.; Chen, P.; Kayed, R.; Glabe, C. G.; Frautschy, S. A.; Cole, G. M. *J. Biol. Chem.* **2005**, *280*, 5892-5901.
(9) Barnham, K. J.; Kenche, V. B.; Ciccotosto, G. D.; Smith, D. P.; Tew, D. J.; Liu, X.; Perez, K.; Cranston, G. A.; Johanssen, T. J.; Volitakis, I.; Bush, A. I.; Masters, C. L.; White, A. R.; Smith, J. P.; Cherny, R. A.; Cappai, R. *Proc. Natl. Acad. Sci. U.S.A.* **2008**, *105*, 6813-6818.
(10) Ehrnhoefer, D. E.; Bieschke, J.; Boeddrich, A.; Herbst, M.; Masino, L.; Lurz, R.; Engemann, S.; Pastore, A.; Wanker, E. E. *Nat. Struct. Mol. Biol.* **2008**, *15*, 558-566.
(11) Sood, A.; Abid, M.; Hailemichael, S.; Foster, M.; Török, B.; Török, M. *Bioorg. Med. Chem. Lett.* **2009**, *19*, 6931-6934.
(12) Cotzias, G. C.; Vanwoert, M. H.; Schiffer, L. M. *N. Engl. J. Med.* **1967**, *276*, 374-379.
(13) Schapira, A. H. V.; Emre, M.; Jenner, P.; Poewe, W. *Eur. J. Neurol.* **2009**, *16*, 982-989.
(14) Kallberg, Y.; Gustafsson, M.; Persson, B.; Thyberg, J.; Johansson, J. *J. Biol. Chem.* **2001**, *276*, 12945-12950.
(15) Nerelius, C.; Sandegren, A.; Sargsyan, H.; Raunak, R.; Leijonmarck, H.; Chatterjee, U.; Fisahn, A.; Imarisio, S.; Lomas, D. A.; Crowther, D. C.; Stromberg, R.; Johansson, J. *Proc. Natl. Acad. Sci. U.S.A.* **2009**, *106*, 9191-9196.
(16) Yu, H.; Li, M.; Liu, G.; Geng, J.; Wang, J.; Ren, J.; Zhao, C.; Qu, X. *Chem. Sci.* **2012**, *3*, 3145-3153.
(17) Rubin, N.; Perugia, E.; Goldschmidt, M.; Fridkin, M.; Addadi, L. *J. Am. Chem. Soc.* **2008**, *130*, 4602-4603.
(18) Howson, S. E.; Bolhuis, A.; Brabec, V.; Clarkson, G. J.; Malina, J.; Rodger, A.; Scott, P. *Nat. Chem.* **2012**, *4*, 31-36.
(19) Hannon, M. J.; Meistermann, I.; Isaac, C. J.; Blomme, C.; Aldrich-Wright, J. R.; Rodger, A. *Chem. Commun.* **2001**, 1078-1079.
(20) Brabec, V.; Howson, S. E.; Kaner, R. A.; Lord, R. M.; Malina, J.; Phillips, R. M.; Abdallah, Q. M. A.; McGowan, P. C.; Rodger, A.; Scott, P. *Chem. Sci.* **2013**, *4*, 4407-4416.
(21) Geng, J.; Li, M.; Ren, J.; Wang, E.; Qu, X. *Angew. Chem. Int. Ed.* **2011**, *50*, 4184 -4188.
(22) Kim, W.; Kim, Y.; Min, J.; Kim, D. J.; Chang, Y.-T.; Hecht, M. H.; *ACS Chem. Biol.* **2006**, *1*, 461-469.
(23) Gao, N.; Sun, H.; Dong, K.; Ren, J.; Duan, T.; Xu, C.; Qu, X. *Nature Commun.* **2014**, *5*, 3422.
(24) Levine, H. *Protein Sci.* **1993**, *2*, 404-410.
(25) Yang, W.; Wong, Y.; Ng, O. T. W.; Bai, L.-P.; Kwong, D. W. J.; Ke, Y.; Jiang, Z.-H.; Li, H.-W.; Yung, K. K. L.; Wong, M. S. *Angew. Chem. Int. Ed.* **2012**, *51*, 1804 -1810.
(26) Cabaleiro-Lago, C.; Quinlan-Pluck, F.; Lynch, I.; Lindman, S.; Minogue, A. M.; Thulin, E.; Walsh, D. M.; Dawson, K. A.; Linse, S. *J. Am. Chem. Soc.* **2008**, *130*, 15437-15443.
(27) Mishra, R.; Bulic, B.; Sellin, D.; Jha, S.; Waldmann, H.; Winter, R. *Angew. Chem. Int. Ed.* **2008**, *47*, 4679-4682.
(28) Sandberg, A.; Luheshi, L. M.; Söllvander, S.; de Barros, T. P.; Macao, B.; Knowles, T. P. J.; Biverstål, H.; Lendel, C.; Ekholm-Petterson, F.; Dubnovitsky, A.; Lannfelt, L.; Dobson, C. M.; Härd, T. *Proc. Natl. Acad. Sci. U.S.A.* **2010**, *107*, 15595- 15600.
(29) Sakono, M.; Zako, T. *FEBS J.* **2010**, *277*, 1348-1358.
(30) Olesen O. F.; Dagø, L. *Biochem. Biophys. Res. Commun.* **2000**, *270*, 62-66.
(31) Bieschke, J.; Herbst, M.; Wiglenda, T.; Friedrich, R. P.; Boeddrich, A.; Schiele, F.; Kleckers, D.; del Aamo, J. M. L.; Grüning, B. A.; Wang, Q.; Schmidt, M. R.; Lurz, R.; Anwy, R.; Schnoeg, S.; Fändrich, M.; Frank, R. F.; Rreif, B.; Günther, S.; Walsh, D. M.; Wanker, E. E. *Nat. Chem. Biol.* **2012**, *8*, 93-101.
(32) Bieschke, J.; Russ, J.; Friedrich, R. P.; Ehrnhoefer, D. E.; Wobst, H.; Neugebauer, K.; Wanker, E. E. *Proc. Natl. Acad. Sci. U.S.A.* **2010**, *107*, 7710-7715.
(33) Li, M.; Yang, X.; Ren, J.; Qu, K.; Qu, X. *Adv. Mater.* **2012**, *24*, 1722-1728.
(34) Li, M.; Shi, P.; Xu, C.; Ren, J.; Qu, X. *Chem. Sci.* **2013**, *4*, 2536-2542.

(35) Qu, X.; Trent, J. O.; Fokt, I.; Priebe, W.; Chaires, J. B. *Proc. Natl. Acad. Sci. U.S.A.* **2000**, *97*, 12032-12037.
(36) Song, G.; Xing, F.; Qu, X.; Chaires, J. B.; Ren, J. *J. Med. Chem.* **2005**, *48*, 3471-3473.
(37) Man, B. Y.-W.; Chan, H.-M.; Leung, C.-H.; Chan, D. S.-H.; Bai, L.-P.; Jiang, Z.-H.; Li, H.-W.; Ma, D.-L. *Chem. Sci.* **2011**, *2*, 917-921.
(38) Sinha, S.; Lopes, D. H. J.; Du, Z.; Pang, E. S.; Shanmugam, A.; Lomakin, A.; Talbiersky, P.; Tennstaedt, A.; McDaniel, K.; Bakshi, R.; Kuo, P.-Y.; Ehrmann, M.; Benedek, G. B.; Loo, J. A.; Klärner, F.-G.; Schrader, T.; Wang, C.; Bitan, G. *J. Am. Chem. Soc.* **2011**, *133*, 16958-16969.
(39) Yu, H.; Ren, J.; Qu, X. *Biophys. J.* **2007**, *92*, 185-191.
(40) Yu, H.; Ren, J.; Qu, X. *ChemBioChem* **2008**, *9*, 879-882.
(41) Schlamadinger, D. E.; Kats, D. I.; Kim, J. E. *J. Chem. Educ.* **2010**, *87*, 961-964.
(42) Puchalski, M. M.; Morra, M. J.; von Wandruszka, R. *Fresenius J. Anal. Chem.* **1991**, *340*, 341-344.
(43) Zhang, H.; Liang, Y.; Tang, X.; He, X.; Bai, D. *Neurosci. Lett.* **2002**, *317*, 143-146.
(44) Kanekiyo, T.; Ban, T.; Aritake, K.; Huang, Z.; Qu, W.; Okazaki, I.; Mohri, I.; Murayama, S.; Ozono, K.; Taniike, M.; Goto, Y.; Urade, Y. *Proc. Natl. Acad. Sci. U.S.A.* **2007**, *104*, 6412-6417.
(45) Fu, Z.; Luo, Y.; Derreumaux, P.; Wei, G. *Biophys. J.* **2009**, *97*, 1795-1803.
(46) LeVine III, H. *Arch. Biochem. Biophys.* **2002**, *404*, 106-115.
(47) Yan, X.; Zhu, P.; Fei, J.; Li, J. *Adv. Mater.* **2010**, *22*, 1283-1287.
(48) Ikeda, M.; Tanida, T.; Yoshii, T.; Hamachi, I. *Adv. Mater.* **2011**, *23*, 2819-2822.
(49) Ma, G.; Huang, F.; Pu, X.; Jia, L.; Jiang, T.; Li, L.; Liu, Y. *Chem. Eur. J.* **2011**, *17*, 11657-11666.
(50) Zhang, X.; Tian, Y.; Li, Z.; Tian, X.; Sun, H.; Liu, H.; Moore, A.; Ran, C. *J. Am. Chem. Soc.* **2013**, *135*, 16397-16409.
(51) Hamley, I. W.; Nutt, D. R.; Brown, G. D.; Miravet, J. F.; Escuder, B.; Rodríguez-Llansola, F. *J. Phys. Chem. B* **2010**, *114*, 940-951.
(52) Scherzer-Attali, R.; Pellarin, R.; Convertino, M.; Frydman-Marom, A.; Egoz-Matia, N.; Peled, S.; Levy-Sakin, M.; Shalev, D. E.; Caflisch, A.; Gazit, E.; Segal, D. *PLoS One* **2010**, *5*, e11101-e11115.
(53) Zagorski, M. G.; Barrow, C. J.; *Biochemistry* **1992**, *31*, 5621-5631.
(54) Vivekanandan, S.; Brender, J. R.; Lee, S. Y.; Ramamoorthy, A. *Biochem. Biophys. Res. Commun.* **2011**, *411*, 312-316.
(55) Trott, O.; Olson, A. J. *J. Comput. Chem.* **2010**, *31*, 455-461.
(56) Massaad, C. A.; Washington, T. M.; Pautler, R. G.; Klann, E. *Proc. Natl. Acad. Sci. U.S.A.* **2009**, *106*, 13576-13581.
(57) Li, F.; Calingasan, N. Y.; Yu, F.; Mauck, W. M.; Toidze, M.; Almeida, C. G.; Takahashi, R. H.; Carlson, G. A.; Beal, M. F.; Lin, M. T.; Gouras, G. K. *J. Neurochem.* **2004**, *89*, 1308-1312.
(58) Riley, D. P. *Chem. Rev.* **1999**, *99*, 2573-2587.
(59) Sompol, P.; Ittarat, W.; Tangpong, J.; Chen, Y.; Doubinskaia, I.; Batinic-Haberle, I.; Abdul, H. M.; Butterfield, D. A.; Clair, D. K. St. *Neuroscience* **2008**, *153*, 120-130.
(60) Doctrow, S. R.; Huffman, K.; Marcus, C. B.; Tocco, G.; Malfroy, E.; Adinolfi, C. A.; Kruk, H.; Baker, K.; Lazarowych, N.; Mascarenhas, J.; Malfroy, B. *J. Med. Chem.* **2002**, *45*, 4549-4558.
(61) Pasternack, R. F.; Halliwell, B. *J. Am. Chem. Soc.* **1979**, *101*, 1026-1031.
(62) Geng, J.; Li, M.; Wu, L.; Ren, J.; Qu, X. *J. Med. Chem.* **2012**, *55*, 9146-9155.
(63) Wu, Y.; Wang, D. *J. Proteome Res.* **2009**, *8*, 436-442.
(64) Arispe, N.; Pollard, H. B.; Rojas, E. *Proc. Natl. Acad. Sci. U.S.A.* **1996**, *93*, 1710-1715.
(65) Arispe, N.; Rojas, E.; Pollard, H. B. *Proc. Natl. Acad. Sci. U.S.A.* **1993**, *90*, 567-571.
(66) Diaz, J. C.; Simakova, O.; Jacobson, K. A.; Arispe, N.; Pollard, H. B. *Proc. Natl. Acad. Sci. U.S.A.* **2009**, *106*, 3348-3353.
(67) Yoo, S. I.; Yang, M.; Brender, J. R.; Subramanian, V.; Sun, K.; Joo, N. E.; Jeong, S.-H.; Ramamoorthy, A.; Kotov N. A. *Angew. Chem. Int. Ed.* **2011**, *50*, 5110–5115.
(68) Mourtas, S.; Canovi, M.; Zona, C.; Aurilia, D.; Niarakis, A.; La Ferla, B.; Salmona, M.; Nicotra, F.; Gobbi, M.; Antimisiaris, S. G. *Biomaterials* **2011**, *32*, 1635–1645.
(69) Cheng, P.-N.; Spencer, R.; Woods, R. J.; Glabe, C. G.; Nowick, J. S. *J. Am. Chem. Soc.* **2012**, *134*, 14179–14184.

Table of Contents